Hyperfine Interact (2016) 237:46
DOI 10.1007/s10751-016-1287-4

# Magnetic and Mössbauer studies of pure and Ti-doped $YFeO_3$ nanocrystalline particles prepared by mechanical milling and subsequent sintering

**N. O. Khalifa[1] · H. M. Widatallah[2] · A. M. Gismelseed[2] · F. N. Al-Mabsali[2] · R. G. S. Sofin[2] · M. Pekala[3]**



**Abstract** Single-phased nanocrystalline particles of pure and 10 % $Ti^{4+}$-doped perovskite-related $YFeO_3$were prepared via mechanosynthesis at 450°C. This temperature is ∼150–350 °C lower than those at which the materials, in bulk form, are normally prepared. Rietveld refinements of the X-ray diffraction patterns reveal that the dopant $Ti^{4+}$ ions prefer interstitial octahedral sites in the orthorhombic crystal lattice rather than those originally occupied by the expelled $Fe^{3+}$ ions. Magnetic measurements show canted antiferromagnetism in both types of nanoparticles. Doping with $Ti^{4+}$ lowers the Néel temperature of the $YFeO_3$ nanoparticles from ∼ 586 K to ∼ 521 K. The $Ti^{4+}$-doped $YFeO_3$ nanoparticles exhibit enhanced magnetization and coercivity but less magnetic hyperfine fields relative to the un-doped nanoparticles. The $^{57}$Fe Mössbauer spectra show ∼ 15 % of the $YFeO_3$ nanoparticles and ∼22 of $Ti^{4+}$-doped $YFeO_3$ ones to be superparamagnetic with blocking temperatures $< 78$ K. The broadened magnetic components in the $^{57}$Fe Mössbauer spectra suggest size-dependent hyperfine magnetic fields at the $^{57}$Fe nuclear sites and were associated with collective magnetic excitations. The $^{57}$Fe Mössbauer spectra show the local environments of the $Fe^{3+}$ ions in the superparamagnetic nanoparticles to be more sensitive to the presence of the $Ti^{4+}$ ions relative to those in the larger magnetic nanoparticles.

**Keywords** Yttrium orthoferrite · Nanocrystalline particles · Mössbauer spectrscopy · Mechanical milling

This article is part of the Topical Collection on *Proceedings of the International Conference on the Applications of the Mössbauer Effect (ICAME 2015), Hamburg, Germany, 13–18 September 2015*

✉ H. M. Widatallah
hishammw@squ.edu.om

[1] Physics Department, Faculty of Science, University of Khartoum, PO Box 321, Khartoum 11115, Sudan

[2] Physics Department, College of Science, Sultan Qaboos University, PO Box 36, Al-Khoudh, Muscat 123, Oman

[3] Chemistry Department, University of Warsaw, 101, PL-02-089 Warsaw, Poland

Published online: 22 February 2016

## 1 Introduction

Yttrium orthoferrite of the composition $YFeO_3$, which adopts a distorted orthorhombic perovskite-related structure (space group *Pnma*), is of interest due to its attractive physical and chemical properties that are associated with a variety of applications including fast latching optical switches, sensors and catalysts [1–7]. The distortion from the ideal cubic perovskite structure is mainly in the dodecahedral A-sites that are occupied by the $Y^{3+}$ ions. The $Fe^{3+}$ ions occupy the octahedral Bsites which are less distorted by virtue of their rotation [8–10]. $YFeO_3$ is an antiferromagnet governed by the super-exchange magnetic interaction existing between two $Fe^{3+}$ ions separated by an $O^{2-}$ ion but the alignment of iron moments is not perfectly antiparallel leading to slight spin canting. This results in a small magnetization giving rise to weak ferromagnetism and the Curie temperature associated with this weak ferromagnetism is $\sim$ 640 K [8–10]. Magnetic and diamagnetic partial cation-substitutions of $Fe^{3+}$ in $YFeO_3$ clearly affect the magnetic properties of the material and have been a matter of intensive investigation for some time [10, 12–14]. For instance doping with low-spin $Mn^{3+}$ was found to lead to spin-reorientation [3]. The conventional solid state synthesis of bulk $YFeO_3$ from $Y_2O_3$ and $Fe_2O_3$ involves the prolong heating of their equimolar mixture at high-temperatures ($\sim$ 1500–1800 K) which often leads to the formation of small $Fe_3O_4$ and $Y_3Fe_5O_{12}$ impurity phases, [15]. The preparation of single-phase pure and nanometer sized $YFeO_3$ at the lower temperatures is possible and, is still, an interesting research topic. For example, the microwave-assisted synthesis of nanocrystalline $YFeO_3$ was reported by Lü et al [15]. The preparation of nanoparticulate $YFeO_3$ by ultrasonic assisted method has also been reported by [16]. Widatallah et al have combined mechanosynthesis and hydrothermal techniques to synthesize cation-doped nanocrystalline materials with perovskite structure at significantly low temperatures relative to those at which the bulk counterparts are normally prepared [17, 18]. Their approach consists of initially doping $\alpha$-$Fe_2O_3$ using hydrothermal synthesis with the chosen cation and subsequently milling a reactants' mixture consisting the doped $\alpha$-$Fe_2O_3$.

In this paper we report on using the mechanical milling route followed by sintering to prepare pure nanocrystalline $YFeO_3$ and $Ti^{4+}$doped-$YFeO_3$ starting from mixtures of $Y_2O_3$ with $\alpha$-$Fe_2O_3$ and $Ti^{4+}$-doped $\alpha$-$Fe_2O_3$ respectively. The structure and magnetic properties of both nanocrystalline materials are investigated using XRD, $^{57}$Fe Mössbauer and magnetometry.

## 2 Experimental

To prepare $YFeO_3$ nanoparticles a 1:1 molar mixture of high purity $Y_2O_3$ and $\alpha - Fe_2O_3$ was milled in air for 60h using a Fritsch Pluverisette -6 milling machine at a ball-to-powder-weight ratio of 15:1 and a milling speed of 300 rpm. The 60 h pre-milled reactants' mixture was subsequently sintered in air at different temperatures (12 h) and slowly-cooled.

As the Y: Fe ratio in $YFeO_3$ is 1:1, it is evident that cation doped $YFeO_3$could be prepared by using either cation doped-$Y_2O_3$ and/or cation-doped $\alpha$-$Fe_2O_3$ in the initial 1:1 molar mixture of the reactants as we have shown elsewhere [17]. Consequently a similar route was used to prepare 10 % $Ti^{4+}$-doped $YFeO_3$nanoparticles starting from a 1:1 molar mixture of high purity $Y_2O_3$ and 10 % $Ti^{4+}$-doped $\alpha$-$Fe_2O_3$ prepared hydrothermally as shown previously [17, 18]. X-ray diffraction (XRD) patterns were recorded using Cu-K$\alpha$ radiation ($\lambda = 1.5406$ Å) with a standard X'Pert PRO PANalytical diffractometer. The structural analysis was performed by subjecting the XRD pattern to Rietveld structural refinement using the program MAUD [19]. The particle size and morphology were

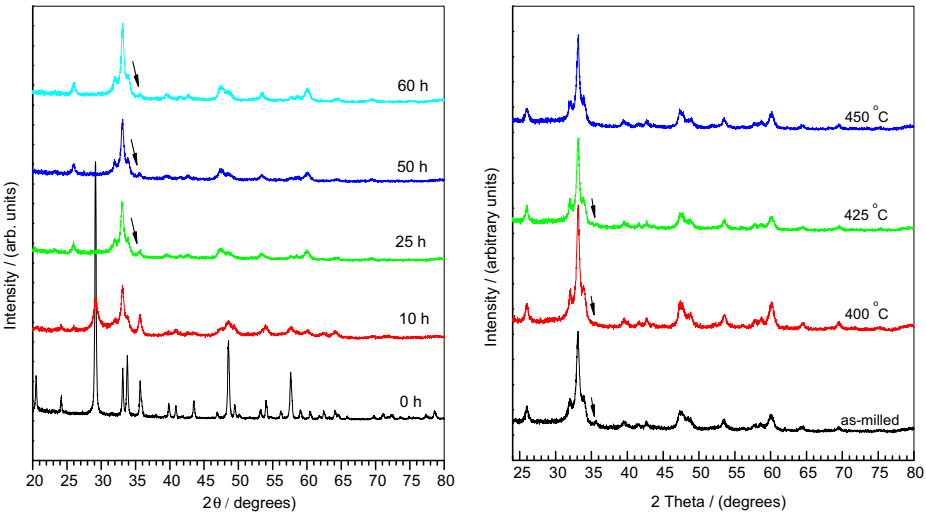


**Fig. 1** The XRD patterns for the 1:1 molar mixture of $Y_2O_3$ and $Ti^{4+}$-doped $\alpha$-$Fe_2O_3$ milled for the times shown; and (right): the XRD patterns for the 60 h pre-milled 1:1 molar mixture of $Y_2O_3$ and $Ti^{4+}$-doped $\alpha$-$Fe_2O_3$ heated (12 h) at the temperature indicated. The arrow shows the most dominant peak of un-reacted $\alpha$-$Fe_2O_3$

determined by transmission electron microscopy (TEM; JEOL 1200EX). Mössbauer measurements were performed on the samples at 300 K and 78 K in a continuous liquid nitrogen flow cryostat using a 25 mCi $^{57}$Co/Rh source with a spectrometer in the transmission mode. The spectrometer was calibrated with $\alpha$-Fe foil spectrum at room temperature. The temperature variation of the magnetization was recorded using a Faraday balance in a magnetic field of 1.5 T at a heating rate of 4 K $min^{-1}$. The field dependence of the magnetization measurement at room temperature was recorded using a commercial vibrating sample magnetometer (VSM) in a magnetic field of up to 1.35 T.

## 3 Result and Discussion

As the evolution of structural phases in both reactants' mixtures evolve in similar ways, it suffices only to discuss the results for one of them. In the Fig. 1 (left) we present XRD patterns collected after subjecting the 1:1 molar mixture of $Y_2O_3$ and Ti-doped $\alpha$-$Fe_2O_3$ to milling for the times shown. It is clear that milling swiftly induces the reaction between $Y_2O_3$ and 10 % Ti-doped $\alpha$-$Fe_2O_3$ (or $\alpha$-$Fe_2O_3$) leading to the formation of a perovskite-related Ti-doped (or pure) $YFeO_3$ phase. The reaction is almost complete after 25 h of milling except for as small amounts of un-reacted $\alpha$-$Fe_2O_3$ as indicated by the presence of its most intense XRD reflection peak at $\sim 35°$ [7]. Further milling for 50 h and 60 h brought about no tangible change in the XRD pattern. In Fig. 1 (right) we present the XRD patterns collected from the 60 h pre-milled 1:1 molar mixture of $Y_2O_3$ and 10 % Ti-doped $\alpha$-$FeO_3$ heated at the temperatures shown (12 h). It is seen that the dominant peak of the un-reacted $\alpha$-$Fe_2O_3$ phase only disappears after heating at 450 °C indicating the formation of single-phased $Ti^{4+}$-doped (or pure) $YFeO_3$. This formation temperature is ∼150–350 °C lower than the temperatures at which the materials, in bulk form, are normally prepared

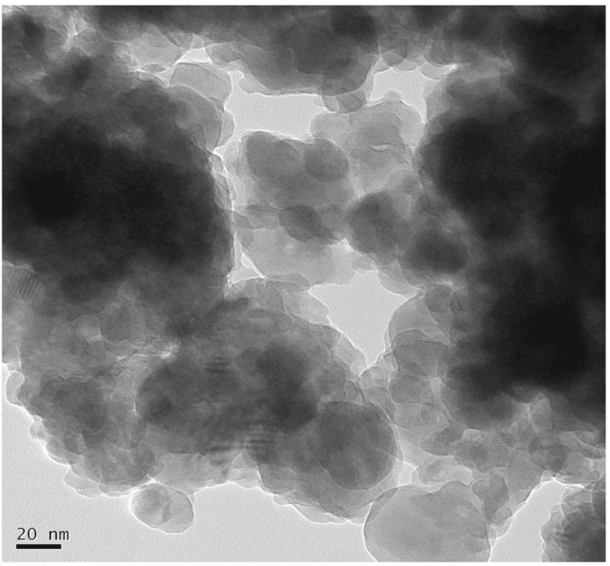


**Fig. 2** The TEM images of the 10 % Ti-doped $YFeO_3$ nanoparticles obtained by heating the 60 h pre-milled 1:1 molar mixture of $Y_2O_3$ and $Ti^{4+}$-doped $\alpha$-$Fe_2O_3$ (12 h) at 450 °C

[13, 15]. The TEM images of the produced materials, shown in Fig. 2 only for the $Ti^{4+}$-doped $YFeO_3$, reveal that both materials are formed of irregularly-shaped nanoparticles with an average size of $\sim$ 35 nm. It is interesting to note that only nanoparticles are formed even though nanoparticles produced via the initial milling of the reactants were sintered at 450 °C for prolonged time (12 h). It is clear that the TEM micrographs show a broad size distribution where single nanoparticles coexist with large interacting nanoparticles' agglomerates.

Using Rietveld structural refinement, the XRD patterns of the 10 % $Ti^{4+}$-doped $YFeO_3$ (Fig. 3 and Table 1) was amenable to satisfactory fitting to a structural model corresponding to a single perovskite-related structure (space group *Pnma* phase). It is seen that 10 % of $Fe^{3+}$ ions are being substituted by 7.5 % $Ti^{4+}$ ions at the octahedral B sites (or the 4b positions in the Wyckoff's notation). These occupancy percentages are consistent with the charge-balance requirement when the trivalent $Fe^{3+}$ ions are replaced by tetravalent $Ti^{4+}$ ions. The lattice parameters obtained for the $Ti^{4+}$-doped $YFeO_3$, namely $a = 5.605$Å, $b = 7.636$Å, $c = 5.301$Å are all larger than those of pure $YFeO_3$, *viz.* $a = 5.5877$Å, $b = 7.5951$Å, $c = 5.2743$Å and reflect the random distribution of the larger octahedral $Ti^{4+}$ radius (74.5 pm) relative to that of the expelled $Fe^{3+}$ (69 pm) as well bond elongation in the surface layers of the particles [20–23]. Our best fit to the experimental XRD data of the $Ti^{4+}$-doped $YFeO_3$ particles show the $Ti^{4+}$ ions to prefer interstitial octahedral sites to those originally occupied by the expelled $Fe^{3+}$ ions.

Figure 4 shows the magnetization versus magnetic field curves recorded at room temperature for both $YFeO_3$ and $Ti^{4+}$-doped $YFeO_3$ nanoparticles. An expanded version of the same plot with the return branches of hysteresis omitted is shown for clarity in the inset of Fig. 4. The magnetization does not saturate even at the highest possible field used (1.35 T). The field-dependent magnetization reveals nearly a line superimposed on a weak-ferromagnetic-like hysteresis loop. The linearity behavior is typical for antiferromagnetic

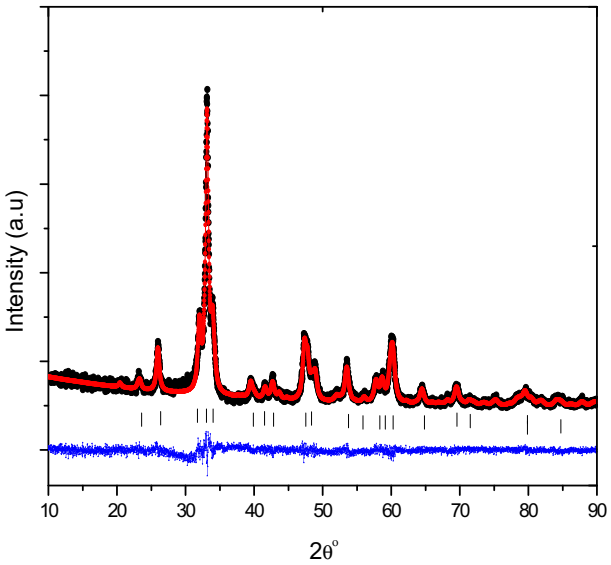


**Fig. 3** The observed (*black dots*), calculated (*solid red line*) and difference XRD patterns (*blue line at the bottom*) for the 10 % Ti-doped $YFeO_3$ nanoparticles obtained at 450 °C. The vertical bars refer to the positions of the Bragg's peaks

materials [24], whereas the hysteresis could be associated with enhanced canted antiferromagnetism at the nanoparticles' surface layers leading to weak ferromagnetism [25]. It is interesting that the Ti-doped $YFeO_3$ nanoparticles exhibit enhanced magnetization relative to the $YFeO_3$ nanoparticles, This could be attributed to an enhanced canting due the presence of both the diamagnetic $Ti^{4+}$ dopant ions and the required $Fe^{3+}$ vacancies to restore charge balance in the lattice, both of which would result in larger spin canting angles. While the remnant magnetization is almost the same for $YFeO_3$ and Ti-doped $YFeO_3$ nanoparticles, the latter shows almost twice the coercivity of the former (0.8 kOe) as is shown in the inset of Fig. 4. This, also, could be related to the presence of uncompensated spins due to the presence of the $Ti^{4+}$ dopant ions and the balancing $Fe^{3+}$ vacancies, which in turn result in frustrated spin systems due to non-collinear magnetic ordering.

Figure 5 shows the temperature variation of the magnetic flux of the $YFeO_3$ and the Ti-doped $YFeO_3$ nanocrystalline particles prepared at 450 °C and a 1.5 T applied field. For both materials the magnetization curve M(T) can be resolved into two components; namely a weak ferromagnetic component $M_F(T)$, and a paramagnetic one, $M_p(T)$. As indicated earlier $M_F(T)$ results from the spin canting associated with the asymmetry in the magnetic unit cell, which is an abruptly decaying function of temperature. The fact that the low temperature magnetization of the doped Ti-doped $YFeO_3$ is higher than that of the $YFeO_3$ could be ascribed to the incomplete antiferromagnetic compensation in the $Fe^{3+}/Ti^{4+}$ sublattice where the antiferromagnetic $Fe^{3+}$-O-$Fe^{3+}$ exchange interaction weakens leading to spin canting relative to the antiferromagnetic axis. This results in an enhanced net magnetization relative to the undoped $YFeO_3$. The Néel temperature, $T_N$, were found to decrease to $\sim$ 586 K for the $YFeO_3$ nanoparticles relative to the corresponding bulk ($\sim$ 640 K). This is clearly a size effect and is associated with expected disorder of the magnetic spins at the surface of the nanoparticles relative to their cores. The Néel temperatures of the Ti-doped $YFeO_3$

**Table 1** Structural parameters obtained from single-phase refinement of 10 % Ti doped-$YFeO_3$ pre-milled for 60 h and heated at 450 °C (12 h) and slowly cooled

| Ion | Wyckoff's position | $x/a$ | $y/b$ | $z/c$ | Occupancy |
|---|---|---|---|---|---|
| $Fe^{3+}$ | 4b | 0.000 | 0.000 | 0.500 | 0.9 |
| $Ti^{4+}$ | 4b | 0.930 | 0.047 | 0.540 | 0.075 |
| $Y^{3+}$ | 4c | 0.068 | 0.250 | 0.978 | 1.0 |
| $O_1^{2-}$ | 4c | 0.457 | 0.250 | 0.114 | 1.0 |
| $O_2^{2-}$ | 8d | 0.694 | 0.932 | 0.289 | 1.0 |

Unit cell Pnma; a=5.605Å, b=7.636 Å, c=5.301 Å; Bragg's R factor: 10.66 %

nanocrystalline particles decrease to ∼ 521 K. Such a decrease in $T_N$ could be attributed to the reduction of the average number of magnetic $Fe^3$-O-$Fe^3$ bonds and the inevitable weakening of the exchange interaction. This, in turn, lowers the internal magnetic energy to offset the antiferromagnetic/weak ferromagnetic spin alignment.

To understand the local environment of iron atoms, the Mössbauer spectra recorded at 300 K and 78 K from the of the $YFeO_3$ and the Ti-doped $YFeO_3$ nanocrystalline particles prepared at 450 °C are shown in Fig. 6. We first discuss the general features of the spectra before relating them to specific phases or structural environments within the nanoparticles. All spectra depict a broad central doublet flanked by a broad six-line magnetic pattern. Each Mössbauer spectrum was best-fitted with a number of magnetic sextets and central doublets whose hyperfine parameters are given in Table 2. The isomer shift values of all spectral components are typical of octahedrally coordinated $Fe^{3+}$ ions [26], indicating that the $Fe^{3+}$ ions in both materials exclusively occupy octahedral sites in consistency with the results of the XRD Rietveld refinement (Table 1).

The broad central doublet in the 300 K and 78 K spectra of the nanocrystalline $YFeO_3$ sample is associated with superparamagnetism due to the smallest single nanoparticles in the sample (Fig. 2). The small volume of these nanoparticles leads the thermal spin fluctuations to overcome the magnetic anisotropy energy that orders the spins. These broad doublets were resolvable into narrower doublets with different values of quadrupole splitting (Table 2) suggesting the presence of varying degrees of structural distortions around the $^{57}$Fe nuclei. Indeed surface effects, such as high strains, which lead to asymmetrical environments around the Mössbauer nuclei, could vary considerably with decreasing size of the nanoparticles. This leads to varying values of extra-nuclear electric field gradients and consequently different quadrupole splitting values. So the quadrupole splitting values in the case of the $YFeO_3$ superparamagnetic particles (Table 2) are indicative of different degrees of crystalline distortion. The larger quadrupole splitting values indicate a more asymmetrical $^{57}$Fe environment which is expected as the nanoparticles' size deceases. The fact the intensity of superparamagnetic doublet remained at ∼ 15 % implies that these nanoparticles have blocking temperatures < 78 K.

It follows from the above, that the broad magnetic components in the 300 K and 78 K Mössbauer spectra of the $YFeO_3$ nanocrystalline sample are associated with the antiferromagnetic ordering in both the large nanoparticles as well as agglomerated grains of interacting nanoparticles. Unlike bulk $YFeO_3$, which exhibits a narrow magnetic sextet [27], the magnetic spectrum of present nanocrystalline $YFeO_3$ sample requires a multitude of sextets to fit. Noting the broad size distribution revealed in Fig. 2, we tend to interpret

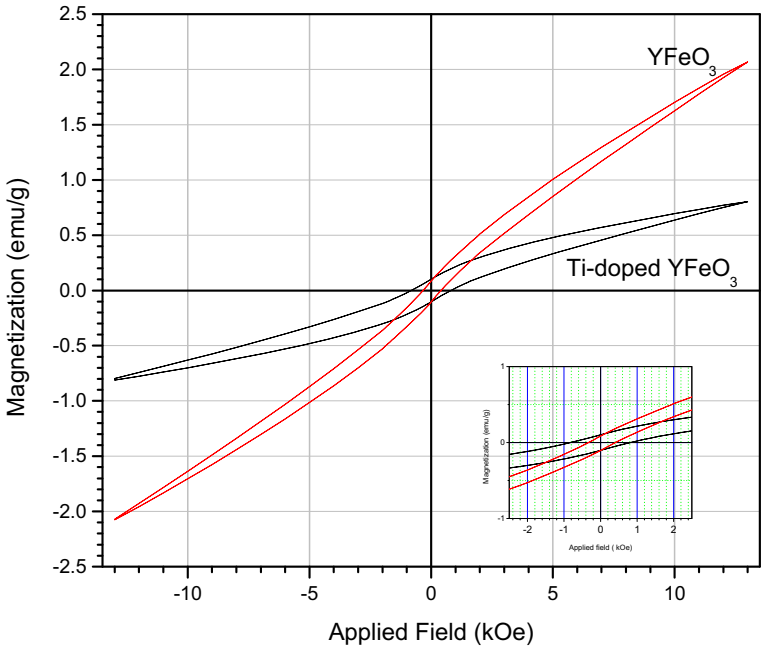


**Fig. 4** Hysteresis loops at room temperature for $YFeO_3$ and the Ti-doped $YFeO_3$ nanocrystalline particles prepared at 450 °C. The inset shows the same hysteresis loops being expanded to show the details in the vicinity of zero field

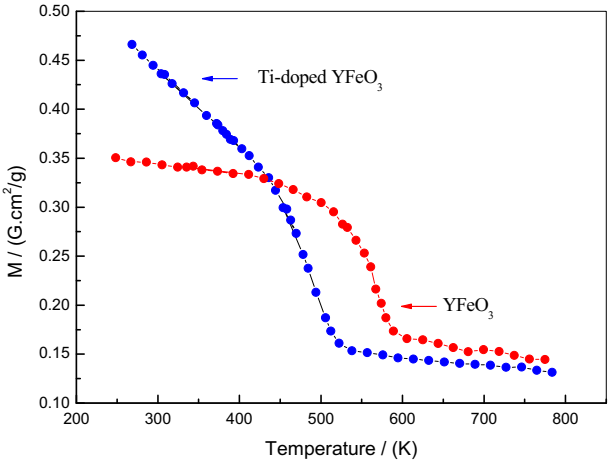


**Fig. 5** The temperature variation of the magnetic flux of the $YFeO_3$ and the Ti-doped $YFeO_3$ nanocrystalline particles prepared at 450 °C at 1.5 T applied field

present data in terms of the collective excitations model [28, 29]. According to this model the magnetization fluctuations, that may be thought of as a combination of precession of the sublattice magnetization vector in the anisotropy field and transitions between precession

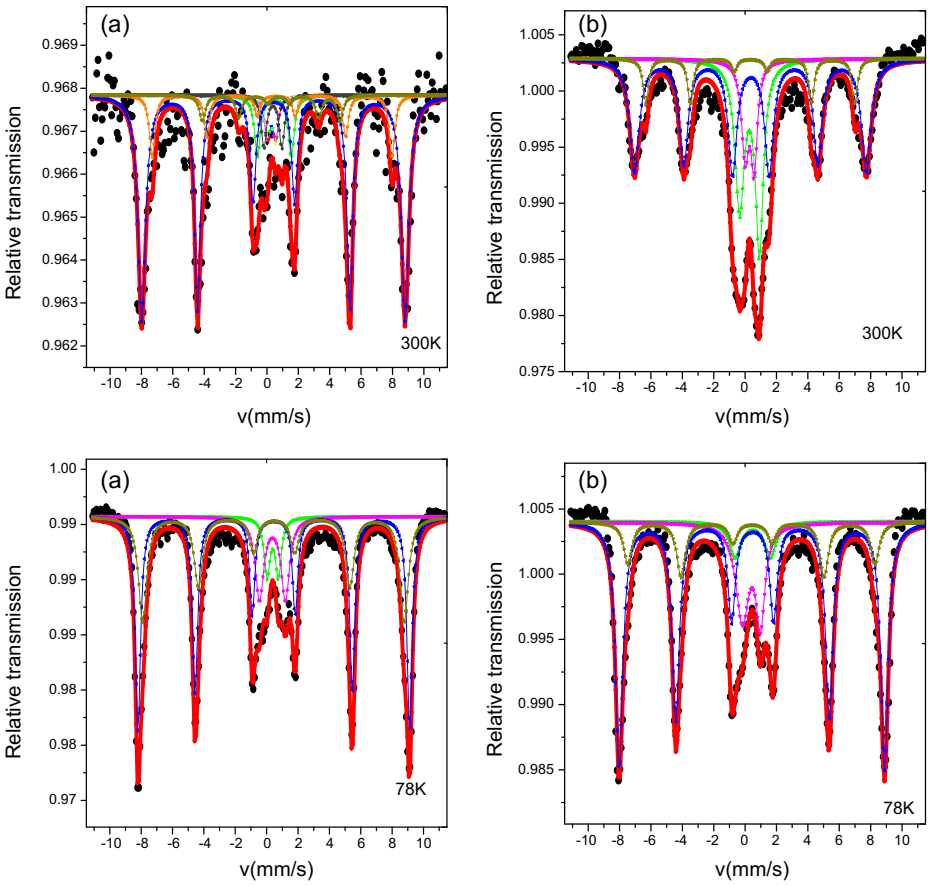


**Fig. 6** The $^{57}$Fe Mössbauer spectra recorded at 300 K and 78 K for (**a**) the $YFeO_3$ and (**b**) 10 % Ti-doped $YFeO_3$ nanoparticles prepared at 450 °C (12) (see text)

states with different precession angles, lead to a particle-size-dependent magnetic hyperfine field. If the correlation time of the collective magnetic excitations is shorter than the time scale of Mössbauer spectroscopy, the measured value of the hyperfine field ($H_{eff}$) will be reduced according to the equation:

$$H_{eff}(V,T) = H_{eff}(V=\infty,T)\left[1-\frac{k_B T}{2KV}\right]$$

where $k_B$ is Boltzmann constant, $V$ the particle volume, $K$ the anisotropy constant, and V = ∞ T refers to a large crystal at temperature $T$ in the absence of collective magnetic excitations. Consequently the hyperfine field decreases with decreasing particle volume. Thus the sextet with high $H_{eff}$ value (Table 2) corresponds to larger nanoparticles and that with low $H_{eff}$ value corresponds to smaller in the sample. The small values of quadrupole shifts of the magnetic components (Table 2) indicate an almost symmetric octahedral environment of the $Fe^{3+}$ ions in the larger "magnetic" particles in the sample.

**Table 2** The Mössbauer spectral parameters of the nanocrystalline $YFeO_3$ and 10 % $Ti^{4+}$ doped -$YFeO_3$ nanoparticles. The best-fitted components should not be taken as corresponding to unique well-defined surroundings, but as representatives of various degrees of structural disorder and different particle sizes as described in the text

| Compound | Temp. (K) | Spectral component | $\delta$ ($\pm$ 0.01 mms$^{-1}$) | QS ($\pm$ 0.01 mms$^{-1}$) | $\Gamma$ ($\pm$ 0.01 mms$^{-1}$) | $H_{eff}$ ($\pm$ 0.1T) | Area ($\pm$ 2 %) |
|---|---|---|---|---|---|---|---|
| $YFeO_3$ | 300 | D1 | 0.48 | 2.15 | 0.23 | | 7 |
| | | D 2 | 0.30 | 0.53 | 0.20 | | 4 |
| | | D 3 | 0.39 | 1.14 | 0.20 | | 5 |
| | | M 1 | 0.43 | −0.01 | 0.22 | 52.0 | 65 |
| | | M 2 | 0.47 | −0.13 | 0.21 | 47.3 | 13 |
| | | M 3 | 0.52 | −0.24 | 0.23 | 27.2 | 6 |
| | 78 | D1 | 0.39 | 0.73 | 0.23 | | 5 |
| | | D 2 | 0.38 | 1.53 | 0.27 | | 10 |
| | | M 1 | 0.45 | 0.00 | 0.20 | 53.7 | 53 |
| | | M 2 | 0.45 | −0.02 | 0.31 | 51.5 | 32 |
| Ti-doped | 300 | D1 | 0.29 | 1.25 | 0.30 | | 25 |
| $YFeO_3$ | | D 2 | 0.30 | 0.57 | 0.23 | | 12 |
| | | M 1 | 0.35 | −0.01 | 0.33 | 46.5 | 53 |
| | | M 2 | 0.36 | −0.01 | 0.20 | 43.1 | 10 |
| | 78 | D1 | 0.49 | 2.25 | 0.42 | | 6 |
| | | D 2 | 0.40 | 1.15 | 0.33 | | 16 |
| | | M 1 | 0.45 | −0.02 | 0.28 | 52.4 | 62 |
| | | M 2 | 0.44 | −0.03 | 0.32 | 48.8 | 16 |

$\delta$: Isomer Shift, QS: Quadrupole splitting/shift, $\Gamma$: FWHM, $H_{eff}$: effective magnetic hyperfine field

We now turn to the Mössbauer spectra recorded at 300 K and 78K for the $Ti^{4+}$-doped $YFeO_3$ nanoparticles (Fig. 6 and Table 2). While the spectra generally bear features similar to those of the pure $YFeO_3$ nanoparticles, they reflect how the $Ti^{4+}$ impurity cations affect the environment of $^{57}$Fe nuclei. As the isomer shift values are typical for the $Fe^{3+}$, we rule out the presence of any $Fe^{2+}$ ions as balancing defects due the incorporation of $Ti^{4+}$ in the $YFeO_3$ structure. This is consistent with the result of the XRD Rietveld refinement, given earlier, that shows the expelled $Fe^{3+}$ ions to be replaced partly by $Ti^{4+}$ ions and no reduction of $Fe^{3+}$ to $Fe^{2+}$ to take place. Unlike in the $YFeO_3$ case, the central superparamagnetic spectral component for the $Ti^{4+}$ in the $YFeO_3$nanoparticles decreases form $\sim$ 37 % at 300 K to $\sim$ 22 % at 78 K. As the size distributions of both nanomaterials are similar, the larger central superparamagnetic spectral component in the 300 K spectrum of the $Ti^{4+}$ -doped $YFeO_3$ nanoparticles relative to that of the $YFeO_3$ nanoparticles - at the same temperature - is clearly not solely due to size effects. Rather it also reflects the presence the non-magnetic $Ti^{4+}$ ions which contribute to lowering the magnetic anisotropy energy relative to the thermal agitation energy through weakening the exchange interactions between magnetic irons.

The hyperfine field values ($H_{eff}$) for the magnetic sextets in the spectra of the Ti-doped $YFeO_3$nanoparticles are lower than those of the non-doped $YFeO_3$ nanoparticles. This, again, suggests that in addition to the particle size effect discussed earlier that leads to

collective magnetic excitations, these reduced $H_{eff}$ could be associated with $Fe^{3+}$ ions having different concentrations of $Ti^{4+}$ cationic neighbors that lead to weaker magnetic exchange magnetic interactions as was mentioned above. This, in turn, results in the observed decrease of the magnetic hyperfine fields relative to those in the non-doped samples. Consequently we associate the sextet with lower $H_{eff}$ with $Fe^{3+}$ ions having a higher concentration of $Ti^{4+}$ neighbors relative to those associated with the higher $H_{eff}$.

It is seen in Table 2 that the mean values of the isomer shift of nanocrysytalline $YFeO_3$ are rather weakly temperature dependent relative to those of nanocrysytalline Ti-doped counterpart. This implies a small second-order Doppler shift between 78 K and 300 K for the former relative to the later. As the second-order Doppler shift depends upon the mean-square velocities of the emitting and absorbing Mössbauer atoms, this could indicate that the mean-square velocities of Fe ions in the Ti-doped sample are higher relative to those of the undoped sample. This could be associated with the presence of the vacant sites due to the presence of the 3 $Ti^{4+}$ dopant ions instead of every 4 $Fe^{3+}$ ions as the Rietveld results of Table 1 indicate. Such vacancies, though few, could slightly relax the stronger bonding in this ionic compound thereby increasing the Fe ionic mean-square displacement and hence their velocities relative to the undoped $YFeO_3$ sample.

A final comment goes to the slight change in the values of the isomer shifts for all doublets that shows the local environments of $Fe^{3+}$ ions, in the superparamagnetic particles, to be sensitive to the presence of the $Ti^{4+}$ ions. By contrast the magnetic sextets exhibit insignificant change of isomer shift values indicating that the s-electron densities at the $^{57}Fe$ nuclei, in the larger particles, are almost unaffected by Ti doping.

**Acknowledgment** One of the authors (NOK) would like to thank the Organization for Women in Science for the Developing world (OWSD) Trieste, Italy, for a research fellowship. Also our thanks are extended to Dr. A. A. Abdalla Dr. R. M. Ibrahim and Dr. I. Riad of Khartoum University, Sudan and Prof. A. D. Al-Rawas of Sultan Qaboos University, Oman for their support.

## References

1. Lima, E., Martins, T.B., Rechenberg, H.R., Goya, G.F., Cavelius, C., Rapalaviciute, R., Hao, S., Mathur, S.: J. Magn. Magn. Mater. **320**, 622 (2008)
2. Shang, M., Zhang, C., Zhang, T., Yuan, L., Ge, L.: H.Yuan, S. Feng. J. Appl. Phys. Lett. **062903**, 102 (2013)
3. Sundarayya, Y., Mandal, P., Sundaresan, A., Rao, C.N.R.: J. Phys.: Condens. Matter. **436001**, 23 (2011)
4. Durbin, G.W., Johnson, C.E., Thomas, M.F.: J. Solid State Phys. **8**, 3051 (1975)
5. Wood, S., Geller, E.A.: J. Acta Cryst. **9**, 563 (1956)
6. Jacob, K.T., Rajitha, G.: J. Solid State Ionics. **224**, 32 (2012)
7. Hui, S., Xu, J., Wu, A.: J. Rare Earths. **28**, 416 (2010)
8. Yang, H., Yang, Y., Lin, Y.: Liu, M. Ceram. Inter. **39**, 235 (2013)
9. Shen, H., Xu, J., Wu, A., Zhao, J., Shi, M.: J. Mater. Sci. Eng. **157**, 77 (2009)
10. Hou, D., Feng, L., Zhang, J., Dong, S., Zhou, D.: Lim, T.-T. J. Hazardous. Mater. **200**, 301 (2012)
11. Gil, D.M., Navarro, M.C., Lagarrigue, M.C., Guimpel, J., Carbonio, R.E., Gomez, M.I.: J. Therm. Anal. Calorim. **103**, 889 (2011)
12. Bolarin, A.M., Snchez-De Jesus, M.F., Cortés-Escobedo, C.A., Valenzuel, R., Ammar, S.: J. Alloy. Comp. **586**, 90 (2014)
13. Yuan, X., Sun, Y., Xu, M.: J. Solid State Chem. **196**, 362 (2012)
14. Shen, H., Xu, J., M. J., Jiang, G.: Ceram. Inter. **38**, 1473 (2012)
15. Lü, X., Xie, J., Shu, H., Liu, J., Yin, C., Lin, J.: Mater. Sci. Eng. B **138**, 289 (2007)
16. Tang, P.S., Tang, C.W., Ying, J.N., Ni, D.J., Yang, Q., Wu, L.M.: Key Eng. Mater. **7**, 636 (2014)
17. Widatallah, H.M., Al-Qayoudhi, M.S., Gismelseed, A., Al-Rawas, A., Al-Harthi, S.H., Khalafalla, M.E.H., Elzain, M., Yousif, A., Al-mari, I.: J. Hyper. Interact. **226**, 143 (2014)

18. Widatallah, H.M., Gismelseed, A.M., Bouziane, K., Berry, F.J., Rawas, A.D., Al-Omari, I.A., Yousif, A.A., Elzain, M.E.: J. Hyper. Interact. **156/157**, 223 (2004)
19. Lutterotti, L.: Res. Nucl. Inst. Methods Phys. B **268**, 334 (2010)
20. Jacoba, K.T., Rajithaa, G., Dasgupta, N.: Ind. J. Eng. Mater. Sci. **19**, 47 (2012)
21. Mathur, S., Veith, M., Rapalaviciute, R., Shen, H., Goya, G.F., Martins Filho, W.L., Berqu, T.S.: J. Chem. Mater. **16**, 1906 (2004)
22. Winter, M.J.: www.webelements.com
23. du Boulay, D., Maslen, E.M., Strltsov, A., Ishizawa, N.: Acta. Cryst. **B51**, 921 (1995)
24. Park, T.-J., Papaefthymiou, G.C., Viescas, A.J., Stanislaus, A.R.M., Wong, S.: Nano Lett. **7**, 776 (2007)
25. Silva, K.L., Menzel, D., Feldhoff, A., KEubel, C., Bruns, M., Paesano, A., Deuvel, A., Wilkening, M., Ghafari, M., Hahn, H., Litterst, F.J., Heitjans, P., Becker, K.D., Sepelak, V.: J. Phys. Chem. C **115L**, 7209 (2011)
26. Qian, Z., Jiang, J.S., Jiang, D.M., Zhang, W.G., Liu, J.H.: J. Phys. D: Appl. Phys. **025403**, 43 (2010)
27. Sundarayya, Y., Mandal, P., Sundaresan, A., Rao, C.N.R.: J. Phys.: Condens. Matter. **436001**, 23 (2011)
28. Tørup, S.M., Tøpsoe, H.: Appl. Phys. **11**, 63 (1976)
29. Mørup, S., Frandsen, C., Bødker, F., Khausen, S.N., Lefmann, K., Lindgard, P.A., Hansen, M.F.: Hyperfine Interact. **144/145**, 347 (2002)